

Orbital angular momentum impact on light scattering by phonons tested experimentally

A. Pylypets, F. Borodavka, I. Rafalovskyi, I. Gregora, E. Buixaderas, P. Bohacek, and J. Hlinka*

FZU - Institute of Physics of the Czech Academy of Sciences

Na Slovance 2, 182 21 Prague 8, Czech Republic

(Dated: October 29, 2024)

Polarized Raman spectra of piezoelectric bismuth germanate single crystal were recorded using vortex light in order to verify the predicted symmetry selection rules for Raman scattering of photons with nonzero orbital angular momentum. At first, the phonon spectrum is fully characterized by the infrared reflectivity and Raman scattering with ordinary light. Then, vortex light Raman spectra were compared with the ordinary ones, but no influence of the orbital momentum on the Raman spectra of $\text{Bi}_4\text{Ge}_3\text{O}_{12}$ was observed. In particular, we experimentally negate the theoretical prediction that Raman scattering using vortex light can yield frequencies of the silent optic modes of $\text{Bi}_4\text{Ge}_3\text{O}_{12}$. We also have not seen evidence for the predicted symmetry-lowering of the Raman scattering tensors of E modes. We propose that the orbital momentum effects are inaccessible to the ordinary Raman spectroscopy experiments because of the tiny magnitudes of typical phonon coherence lengths.

Is photon scattering by lattice vibrations in crystals sensitive to the orbital angular momentum of light? The clearly formulated relationship between the spin and the internal orbital momentum of light and the availability of the beams with quantized orbital angular momentum (OAM) have brought novel opportunities for light-matter interaction experiments [1, 2]. In particular, Laguerre-Gaussian beam with an azimuthal phase dependence $e^{im\phi}$, where ϕ is the azimuthal angle in the beam cross-section and the integer $m \geq 2$ defines the $L = m\hbar$ OAM per photon, can be obtained in the laboratory conditions by passing the basic monochromatic Gaussian mode of the laser beam through a helical phase-shift plate. The helicity of the phase front, its on-axis phase singularity and the annular character of the cross-sectional intensity pattern are topologically protected properties of vortex beams that should persist no matter how tightly the beam is focused. Laguerre-Gaussian and similar optical vortex beams carrying OAM are now applied for example as optical tweezers, in quantum computation or optical communication cryptography [3–7].

Among many other interesting vortex-light effects [8–15], it has been also proposed that Laguerre-Gaussian beams can be used in the inelastic light scattering by phonon modes in crystal lattices (see Fig. 1a). It was argued that scattering by vortex beams with $m \geq 2$ should increase the scattering intensity and the scattering processes should obey different symmetry selection rules than those of the usual Raman scattering of $m = 0$ photons [16, 17]. Specifically, authors of Ref. 16 proposed that Raman scattering tensors of E and A_2 modes of the cubic piezoelectric crystal of $\text{Bi}_4\text{Ge}_3\text{O}_{12}$ (BGO) have additional components that might be comparable to if not larger than those of the ordinary Raman process. In particular, scattering by $m \geq 2$ photons should reveal the Raman-inactive A_2 phonon modes. Obviously, this would be very useful as such silent zone

center modes are otherwise inaccessible to the standard laboratory techniques.

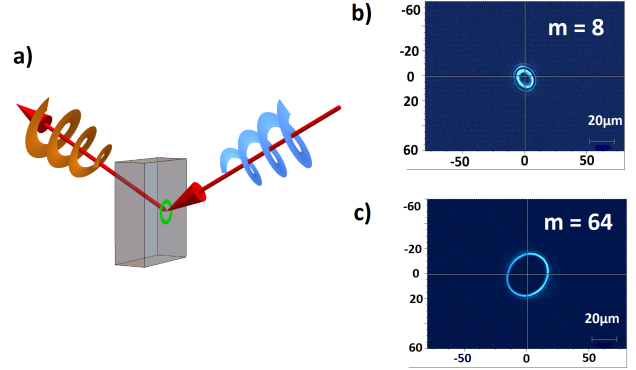


FIG. 1. Raman scattering by vortex light. (a) Illustration of a plausible scattering process preserving the photon orbital momentum, (b) detected scattering ring at the sample surface irradiated by the light beam with $m = 8$ in our experiment and (c) the same for the vortex light with $m = 64$.

The above mentioned theory implies that the OAM of visible light should influence scattering of vortex beam by thermal vibrations in regular crystals. In this paper, we have tested these predictions experimentally. We have first performed a systematic IR and polarization-dependent Raman scattering investigations of the phonon spectra on two single crystals with the usual $m = 0$ light in order to verify to which extent the ensemble of the Raman active modes obeys the classical selection rules. Subsequently, we have tested the predicted influence of the photon OAM on the Raman scattering process in several independent scattering geometries. A clear negative experimental result is obtained in all cases. Finally, a possible reason for the failure of the theory is proposed.

The $\text{Bi}_4\text{Ge}_3\text{O}_{12}$ crystal is known for its outstanding

Label	\mathbf{e}_i	\mathbf{e}_o	surface	active modes
HV(110)	$[\bar{1}\bar{1}0]$	$[001]$	(110)	$F_2(\text{TO})$
HV(001)	$[100]$	$[010]$	(001)	$F_2(\text{LO})$
HV(001)*	$[\bar{1}\bar{1}0]$	$[110]$	(001)	E
VV(001)*	$[110]$	$[110]$	(001)	$A_1 + E + F_2(\text{LO})$
VV(001)	$[100]$	$[010]$	(001)	$A_1 + E$

TABLE I. Convenient back-scattering geometries and symmetry selection rules for the optic modes in the $\bar{4}3m$ symmetry crystal.

photorefractive, scintillating and electrooptic properties [14, 18, 19, 21–23]. In visible spectral range, the pure $\text{Bi}_4\text{Ge}_3\text{O}_{12}$ is a highly transparent material with practically no photoluminescence [24]. It grows in cubic structure described by space group No. 220 $I\bar{4}3d$ (T_d^6) [20]. Its 38 atoms in a primitive cell yield 111 optical branches. The $4A_1 + 5A_2 + 9E + 14F_1 + 14F_2$ optic modes include 14 infrared active ones (F_2) and 27 Raman active ones (A_1, E, F_2). Corresponding Raman tensors are explicitly given e.g. in Ref. 25–27. Relative weights of these modes in the spectrum can be tuned by the polarization of the incident photon (\mathbf{e}_i) and the outgoing scattered photon (\mathbf{e}_o). Convenient geometries allowing to identify the symmetry of the observed modes are listed in Table I. Spectroscopic VV and VH labels derived from the vertical and horizontal photon polarization refer to the usual photon spin conserved and photon spin rotated scattering geometry indicated in the table.

In our experiments, we have used suitably oriented and polished $\text{Bi}_4\text{Ge}_3\text{O}_{12}$ samples made from 1 mm thick crystal substrates (purchased from Alineason company) and cylindrical pieces (13 mm diameter, 10 mm in height) made from crystals grown by Czochralski method in our Institute as in Ref. 24. Samples from both sources had equivalent properties.

The Raman scattering measurements were carried out using a Renishaw Raman microscope operated with a 514 nm Argon laser in forward and back-scattering geometry. The standard setup was supplemented by external rotational stages allowing to perform Raman scattering polarimetry [26–28]. The OAM has been introduced using an optical vortex plate manufactured by HOLO/Or company for the given combination of $m \geq 2$ and the 514 nm wavelength by etching a precise helical profile to a 3 mm-thick fused silica disk. For example, when using an objective with a working distance of 21 mm and 20 \times magnification and placing the vortex plate in the expanded incoming laser beam of diameter about 7 mm, the typical vortex ring intensity obtained at the sample had a diameter of about 15 and 35 μm in case of $m = 8$ and $m = 64$, respectively (see Fig. 1bc). Complementary IR reflectivity spectra were collected using a Fourier-transform Bruker spectrometer IFS 113/V.

Our room-temperature infrared spectra are shown in

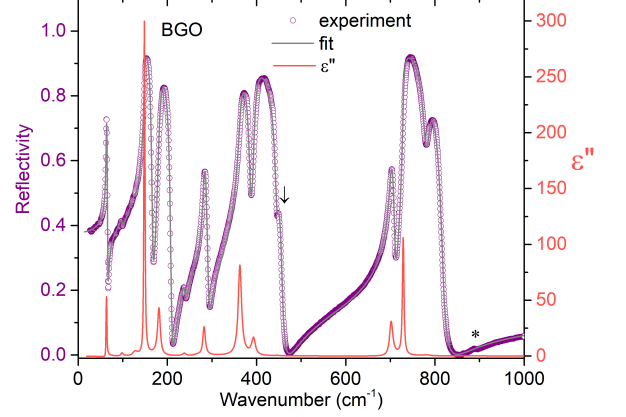


FIG. 2. Normal incidence IR reflectivity spectrum of BGO single crystal at ambient temperature (left scale) with superposed dielectric loss function (right scale) derived by fitting to the standard factorized damped harmonic model. High-frequency permittivity $\epsilon_\infty = 4.335$ agreed with Refs. 21–23. The star symbol is marking a second-order feature at about double frequency compared to that of the weak but clear F_2 mode marked by the arrow.

Fig2. The reflectivity spectrum was fitted to a standard factorized formula [29–31] describing the contribution from the 14 expected damped harmonic oscillators in order to obtain the LO and TO frequencies. In particular, in addition to F_2 modes observed in Refs. 31 and 32, our data show also a clear signature of the sharp F_2 mode near 449 cm^{-1} . A trace of the remaining missing mode near 267 cm^{-1} becomes apparent from the Kramers-Kronig analysis.

As already mentioned, the Raman active modes can be identified using selection rules listed in Table I. In particular, the frequencies of $F_2(\text{TO})$ and $F_2(\text{LO})$ accessed from Raman spectra shown in Fig. 3a are in a very good agreement with infrared data. The modes of A_1 symmetry are known to dominate in parallel-polarized spectra recorded from the (111) surface of the crystal [26, 27], while E modes can be detected for example in the HV(001)* scattering geometry (see Fig. 3b). The list of our mode frequencies is summarized in Table II. The obtained spectrum completes the previous results [32–34] and it is also consistent with the DFT calculation of Ref. 35 apart from acceptable systematic frequency shifts of the order of 10 percent.

The expected m -dependence of the Raman scattering with \mathbf{e}_i and \mathbf{e}_o within (001) plane (evaluated as in Ref. 25 and 27 using tensors of Ref. 16) is shown in Fig. 5 for parallel and crossed polarizer configurations. The vortex light effects concern only the A_2 and E -symmetry modes (the two middle column panels of Fig. 5). We have recorded spectra with the vortex plate in the incoming

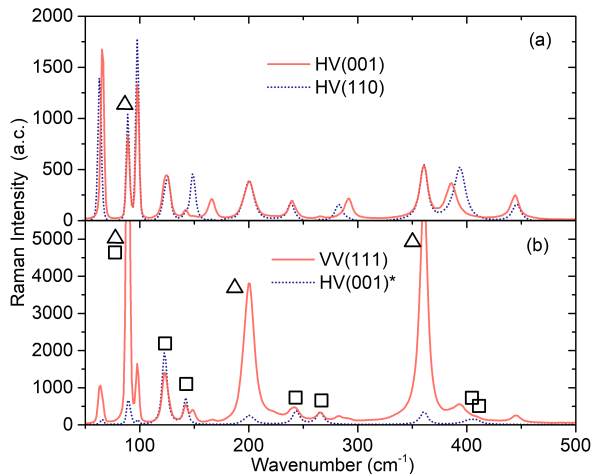


FIG. 3. Back-scattering Raman spectra of BGO at ambient temperature. Cross-polarized spectra in the top panel (a) reveals $F_2(\text{TO})$ phonon modes detected in HV(110) geometry (dotted line) and $F_2(\text{LO})$ in the HV(001) geometry (full line). Triangle marks the leaking A_1 mode. Bottom panel (b) shows parallel-polarized Raman spectrum taken from the (111) surface and cross-polarized Raman spectrum taken from the (011) surface (full and dotted line, resp.). Triangle symbols mark the A_1 symmetry modes, squares are denoting the main E symmetry modes.

No.	$F_2(\text{TO})$	$F_2(\text{LO})$	A_1	E
1	64	66	90	90
2	98	98	201	123
3	124	124	361	142
4	149	166	816	244
5	180	209		266
6	240	240		403
7	266	266		409
8	283	291		719
9	363	387		816
10	394	445		
11	446	460		
12	702	711		
13	730	780		
14	783	818		

TABLE II. Room temperature optic mode frequencies of BGO as determined from the present experiments. Tabulated values are linear wavenumbers in cm^{-1} ($1 \text{ cm}^{-1} \sim 0.030 \text{ THz} \sim 0.124 \text{ meV}$).

laser beam for all polarization combinations listed in Table I. However, no systematic spectral changes were detected. We neither see spectral changes due to vortex light when these experiments were carried out at 5 K, nor when measuring the spectra of Si, TiO_2 or SrTiO_3 single crystals. At the same time, we have recorded the full angular dependence of VV and VH spectra and ver-

ified that within the precision of the experiment, mode intensities perfectly agrees with the standard $m = 0$ prediction (compare Fig. 4 and Fig. 5).

Therefore, we have then focused our efforts on predictions of Ref. 16, specific solely to the A_2 modes. BGO has 5 A_2 modes and so the most revealing result would be the appearance of these otherwise infrared and Raman inactive modes. These modes should appear in VV(001) polarization in case of $m \geq 2$ light. Corresponding back-scattering spectra are shown in Fig. 6. Within our precision and sensitivity, no spectral anomaly was observed.

We have also tried focusing vortex light with objectives of different focal length (*e.g.*, 0.5 mm instead of 21 mm) or with the vortex filter placed after the objective or before the beam expander. On the top of it, we have carried out this key experiment also in forward scattering geometry, when bringing the incoming vortex beam through a 1 mm thick BGO sample. In this case, there are actually few additional modes in the spectrum compared to the forward scattering (Fig. 6). However, the comparison with the Table I shows that these are the F_2 modes and their contribution can be well explained by the fact that in this case our incoming beam was partly depolarized by several additional mirrors in the optical path. In summary, we have to conclude that there is no indication of the predicted activation of A_2 modes and no evidence for novel components of E mode tensors either.

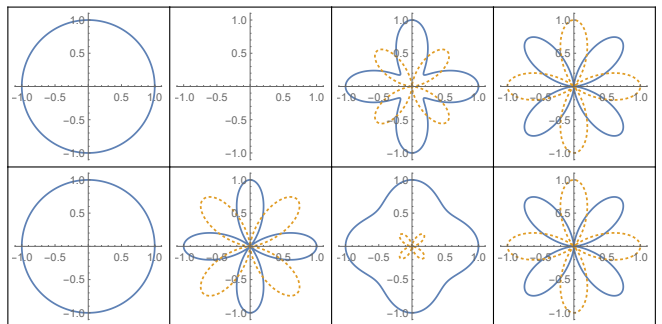


FIG. 4. Expected angular dependence of Raman scattering intensity as a function of the angle between the incoming beam polarization direction \mathbf{e}_i and the (100) crystallographic axis assuming that both \mathbf{e}_i and \mathbf{e}_o are within the (001) plane. From left to right, the panels correspond to the A_1 , A_2 , E and F_2 modes. Top row is for the $m = 0$ scattering, bottom row is for the $m \geq 2$ scattering. Full and dashed line correspond to VV and HV scattering configuration. Intensities are scaled so that maximum value in the panel is equal to 1. The $m \geq 2$ polar plot for the E -mode assumes the particular choice of Raman tensor considered in Ref. 16.

Finally, we have attempted to find out what is the reason for our negative experimental result by inspecting the assumptions made in Ref. 16. The Clebsch-Gordan coefficients approach [36] is an exact method and also the estimations of electronic transition moments appear adequate. Nevertheless, there is perhaps one unwarranted

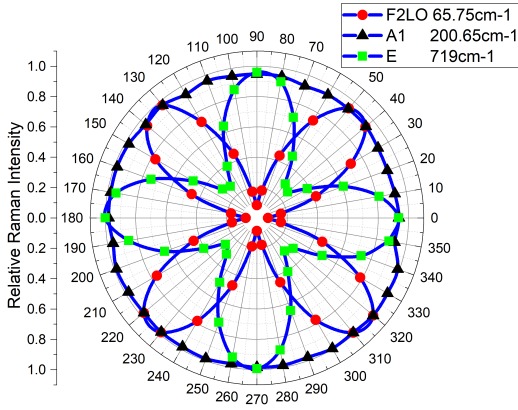


FIG. 5. Experimental parallel-polarized Raman intensity of selected modes as a function of the angle between \mathbf{e}_i and the (100) crystallographic axis. Observed intensities (point symbols) are divided by the maximal detected value. Lines are guides for the eye.

tacit assumption in the theory: the transfer of the orbital momentum to the inelastically scattered photon assumes that the phonon involved is coherent across the vortex beam diameter as well. At the same time, it is known that coherence length of thermal phonons in crystal lattices is typically of the order of 1 nm. Within the Debye approximation, the square of the correlation length in a perfect crystal is equal to the logarithmic derivative of the phonon frequency squared with respect to the square of the phonon momentum. Even the soft phonon correlation lengths near second-order phase transitions are thus only of about 5-10 nm [37–39]. This is far too small in comparison with the diameter of the vortex beam ring. Therefore, we are convinced that the contribution of the individual nanoscale areas on the focused vortex ring should sum up incoherently and the information about the phase integral over the ring is then lost. In other words, the phonon is “too small” and the reason for the insensitivity to the OAM is in principle the same as in the case of interaction with individual atoms [40]. Consequently, the OAM of the photon is not conserved in the Raman process, and the scattered beam is expected to have $m = 0$. Overall, the OAM is probably transferred to the body of the crystal as in the experiment of Ref. 2.

For visible light, the diffraction limit prevents us from making the diameter of the vortex beam comparable to that of the phonon coherence length. In the far-field limit the usual Raman scattering rules fail even in the case of $m = 0$. To our best knowledge, an optical beam carrying a nanoscale vortex lattice is not available[41]. Perhaps, the predicted selection rules are applicable for the soft X-ray vortex Raman scattering. Alternatively, it might be possible to generate coherent A_2 modes by methods based on ultrashort laser pulses similar to the impulsive

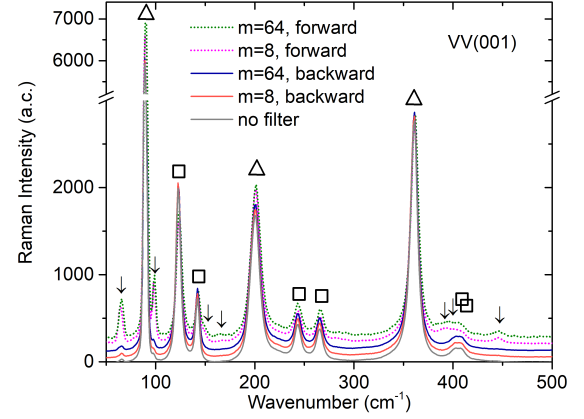


FIG. 6. Parallel-polarized Raman spectra measured in normal incidence at the (001) surface of BGO single crystal with incoming light of variable topological charge m . Individual spectra were normalized to the intensity of strongest A_1 mode near 90 cm⁻¹ and then, for a better visibility, a small vertical offset was applied. From top to bottom, the spectra correspond to near forward scattering with $m = 64$, backward scattering with $m = 64$, backward scattering with $m = 8$, and backward scattering with $m = 0$, respectively. Triangle and square symbols mark the A_1 and E modes, respectively. The only extra peaks located at F_2 mode frequencies arise due to the nonzero xy tensor element of the z -components of the polar phonon modes involved in the near-forward scattering of the incident light in the leaking polarization channel (features marked by arrows).

stimulated Raman scattering [42] and then probing them by OAM light. So far, testing these ideas is an outstanding technical challenge far beyond the scope of the present paper.

In summary, the present work reveals the existence of a substantial obstacle for detecting the OAM-dependent part of the inelastic scattering of light by thermal vibrations of crystals. In particular, it provides a theoretical argument and an experimental evidence against the possibility to detect in the ordinary Raman scattering experiments the neatly formulated theoretical conjectures of Ref. 16. Still, the phonon correlation length argument gives us a possibility that the vortex-light Raman scattering theory can be applied for soft X-ray vortex Raman scattering, or to Raman scattering by coherently excited silent modes. Last but not least, it would be also interesting to extend these considerations to the Raman scattering by magnetic excitations and by low-dimensional materials as proposed in Ref. 17. We hope that our work will bring a valuable new perspective to the ongoing debate[43–47] about various aspects of the interaction of crystalline matter and vortex light beams.

This work was supported by the Czech Science Foundation (project no. 19-28594X) and by the Euro-

pean Union's Horizon 2020 research and innovation programme under grant agreement no. 964931 (TSAR).

* Corresponding author. Email: hlinka@fzu.cz

- [1] M. Padgett, J. Courtial, and L. Allen, Light's orbital angular momentum, *Phys. Today* **57**, 35 (2004).
- [2] L. Allen, M. W. Beijersbergen, R. J. C. Spreeuw, and J. P. Woerdman, Orbital angular momentum of light and the transformation of Laguerre-Gaussian laser modes, *Phys. Rev. A* **45**, 8185 (1992).
- [3] L. Paterson, M. P. MacDonald, J. Arlt, W. Sibbett, P. E. Bryant, and K. Dholakia, Controlled rotation of optically trapped microscopic particles, *Science* **292**, 912 (2001).
- [4] A. Ashkin, J. M. Dziedzic, J. E. Bjorkholm, and S. Chu, Observation of a single-beam gradient force optical trap for dielectric particles, *Optics Lett.* **11**, 288 (1986).
- [5] J. E. Molloy and M. J. Padgett, Lights, action: Optical tweezers, *Contemporary Physics* **43**, 241, (2002).
- [6] M. J. Padgett, Orbital angular momentum 25 years on [Invited], *Opt. Express* **25**, 11265 (2017).
- [7] M. Mirhosseini, O. S. Magaña-Loaiza, M. N. O'Sullivan, B. Rodenburg, M. Malik, M. P. J. Lavery, M. J. Padgett, D. J. Gauthier, and R. W. Boyd, High-dimensional quantum cryptography with twisted light, *New J. Phys.* **17**, 033033 (2015).
- [8] F. Cardano, E. Karimi, S. Slussarenko, L. Marrucci, C. de Lisio, and E. Santamato, Polarization pattern of vector vortex beams generated by q -plates with different topological charges, *Applied Optics* **51**, C1 (2012).
- [9] K. A. Forbes, Raman optical activity using twisted photons, *Phys. Rev. Lett.* **122**, 103201 (2019).
- [10] L. Marrucci, C. Manzo, and D. Paparo, Optical spin-to-orbital angular momentum conversion in inhomogeneous anisotropic media, *Phys. Rev. Lett.* **96**, 163905 (2006).
- [11] L. Ye, L. Yang, X. Zheng, and S. Mukamel, Enhancing circular dichroism signals with vector beams, *Phys. Rev. Lett.* **126**, 123001 (2021).
- [12] P. Salamon, N. Éber, Y. Sasaki, H. Orihara, Á. Buka, and F. Araoka, Tunable optical vortices generated by self-assembled defect structures in nematics, *Phys. Rev. Appl.* **10**, 044008 (2018).
- [13] A. A. Sirenko, P. Marsik, C. Bernhard, T. N. Stanislavchuk, V. Kiryukhin, and S.-W. Cheong, Terahertz vortex beam as a spectroscopic probe of magnetic excitations, *Phys. Rev. Lett.* **122**, 237401 (2019).
- [14] T. T. Fernandez, K. Privat, M. J. Withford, and S. Gross, Record-high positive refractive index change in bismuth germanate crystals through ultrafast laser enhanced polarizability, *Sci. Rep.* **10**, 15142 (2020).
- [15] X. Yi, Y. Liu, X. Ling, X. Zhou, Y. Ke, H. Luo, S. Wen, and D. Fan, Hybrid-order Poincare sphere, *Phys. Rev. A* **91**, 023801 (2015).
- [16] J. Li, J. J. Tu, and J. L. Birman, Raman scattering using vortex light, *J. Phys. Chem. Solids* **77**, 117 (2015).
- [17] R. Saito, M. S. Ukhtary, S. Wang, and N. T. Hung, Selection rule for Raman spectra of two-dimensional materials using circularly-polarized vortex light, *Physical chemistry chemical physics: PCCP*, **23**, 17271 (2021).
- [18] J. Gironnet, V. B. Mikhailik, H. Kraus, P. de Marcillac, and N. Coron, Scintillation studies of $\text{Bi}_4\text{Ge}_3\text{O}_{12}$ (BGO) down to a temperature of 6 K, *Nucl. Instrum. Methods Phys. Res. Sec. A* **594**, 358 (2008).
- [19] M. Nikl, Scintillation detectors for x-rays, *Meas. Sci. Technol.* **17**, R37 (2006).
- [20] A. Grzechnik, $\text{Bi}_4\text{Ge}_3\text{O}_{12}$ at the onset of pressure-induced amorphization, *Acta Cryst. C*, **65**, 63 (2009).
- [21] J. Link, J. Fontanella, and C. G. Andeen, Temperature variation of the dielectric properties of bismuth germanate and bismuth germanium oxide, *J. Appl. Phys.* **51**, 4352 (1980).
- [22] P. A. Williams, A. H. Rose, K. S. Lee, D. C. Conrad, G. W. Day, and P. D. Hale, Optical, thermo-optic, electro-optic, and photoelastic properties of bismuth germanate ($\text{Bi}_4\text{Ge}_3\text{O}_{12}$), *Appl. Optics* **35**, 3562 (1996).
- [23] G. Montemezzani, St. Pfändler, and P. Günter, Electro-optic and photorefractive properties of $\text{Bi}_4\text{Ge}_3\text{O}_{12}$ crystals in the ultraviolet spectral range, *J. Opt. Soc. Am. B* **9**, 1110 (1992).
- [24] M. J. Weber and R. R. Monchamp, Luminescence of $\text{Bi}_4\text{Ge}_3\text{O}_{12}$ -spectral and decay properties, *J. Appl. Phys.* **44**, 5495 (1973).
- [25] I. Gregora, *Raman scattering*, Part of the International tables for crystallography. Vol. D, *Physical properties of crystals*. (ed. A. Authier) 314–328 (Springer Netherlands, Dordrecht, 2003).
- [26] J. Hlinka, F. Borodavka, I. Rafalovskyi, Z. Docekalova, J. Pokorny, I. Gregora, V. Tsurkan, H. Nakamura, F. Mayr, C. A. Kuntscher, A. Loidl, S. Bordács, D. Szaller, H.-J. Lee, J. H. Lee, and I. Kezsmarki, Lattice modes and the Jahn-Teller ferroelectric transition of GaV_4S_8 , *Phys. Rev. B* **94**, 060104(R) (2016).
- [27] K. Tesar, I. Gregora, P. Beresova, P. Vanek, P. Ondrejčokovic, and J. Hlinka, Raman scattering yields cubic crystal grain orientation, *Sci. Rep.* **9**, 9385 (2019).
- [28] I. Rafalovskyi, M. Guennou, I. Gregora, and J. Hlinka, Macroscopic lamellar heterophase pattern in $\text{Pb}(\text{Mg}_{1/3}\text{Nb}_{2/3})\text{O}_3$ – PbTiO_3 single crystals, *Phys. Rev. B* **93**, 064110 (2016).
- [29] D. W. Berreman and F. C. Unterwald, Adjusting Poles and Zeros of Dielectric Dispersion to Fit Reststrahlen of PrCl_3 and LaCl_3 , *Phys. Rev.* **174**, 791 (1968).
- [30] F. Gervais, *Infrared and Millimeter Waves*, edited by K. J. Button (Academic Press, New York, 1983), Chap. 7, p. 279.
- [31] H. F. Haneef and N. J. Podraza, Optical properties of single crystal $\text{Bi}_4\text{Ge}_3\text{O}_{12}$ from the infrared to ultraviolet, *J. Appl. Phys.* **116**, 163507 (2014).
- [32] M. Couzi, J. R. Vignalou, and G. Boulon, Infrared and Raman study of the optical phonons in $\text{Bi}_4\text{Ge}_3\text{O}_{12}$ single crystal, *Solid State Comm.* **20**, 461 (1976).
- [33] B. Mihailova, D. Toncheva, M. Gospodinov, and L. Konstantinov, Raman spectroscopic study of Mn-doped $\text{Bi}_4\text{Ge}_3\text{O}_{12}$, *Solid State Commun.* **112**, 11 (1999).
- [34] P. Beneventi, D. Bersani, P. P. Lottici, and L. Kovács, A Raman study of $\text{Bi}_4(\text{Ge}_x\text{Si}_{1-x})_3\text{O}_{12}$ crystals, *Solid State Commun.* **93**, 143 (1995).
- [35] N. M. Avram, V. A. Chernyshev, E.-L. Andreici, V. P. Petrov, and P. Petkova, Phonon spectra of eulytite crystals $\text{Bi}_4\text{M}_3\text{O}_{12}$ ($\text{M} = \text{Ge}, \text{Si}$): *ab initio* study, *Optical Materials* **61**, 30 (2016).
- [36] J. L. Birman and R. Berenson, Scattering tensors and Clebsch-Gordan coefficients in crystals, *Phys. Rev. B* **9**, 4512 (1974).
- [37] G. Shirane, R. A. Cowley, M. Matsuda, and S. M.

- Shapiro, q dependence of the central peak in the inelastic-neutron-scattering spectrum of SrTiO_3 , *Phys. Rev. B* **48**, 15 595 (1993).
- [38] J. Hlinka, R. Currat, M. de Boissieu, F. Livet, and Yu. M. Vysochanskii, Two-length-scale behavior near the ferroelectric phase transition of $\text{Sn}_2\text{P}_2\text{S}_6$, *Phys. Rev. B* **71**, 052102 (2005).
- [39] J. Hlinka and P. Marton, Phenomenological model of a 90° domain wall in BaTiO_3 -type ferroelectrics, *Phys. Rev. B* **74**, 104104 (2006).
- [40] F. Giammanco, A. Perona, P. Marsili, F. Conti, F. Fidecaro, S. Gozzini, and A. Lucchesini, Influence of the photon orbital angular momentum on electric dipole transitions: negative experimental evidence, *Optics Letters* **42**, 219 (2017).
- [41] P. Salamon, N. Eber, Y. Sasaki, H. Orihara, Á. Buka and F. Araoka, Tunable Optical Vortices Generated by Self-Assembled Defect Structures in Nematics, *Phys. Rev. Appl.*, **10**, 044008 (2018).
- [42] Z. Chen, Y. Gao, B. C. Minch, and M. F. DeCamp, Coherent optical phonon generation in $\text{Bi}_4\text{Ge}_3\text{O}_{12}$, *J. Phys.: Condens. Matter* **23**, 385402 (2011).
- [43] Y. M. Lei, Q. Q. Yang, Z. H. Tang, G. Tian, Z. P. Hou, and M. H. Qin, Rotational motion of skyrmion driven by optical vortex in frustrated magnets, *Applied Physics Letters* **125** 072401 (2024).
- [44] L. Gao, S. Prokhorenko, Y. Nahas, and L. Bellaiche, Effective gyration of polar vortex arrays controlled by high orbital angular momentum of light, *Phys. Rev. B* **109**, L121110 (2024).
- [45] B. Z. Rameshti, S. M. Tabatabaei, and R. A. Duine, Twisted dynamics in magnetic insulators with structured light *Phys. Rev. B* **110** 094437 (2024).
- [46] S. H. Guan, Y. Liu, Z. P. Hou, D. Y. Chen, Z. Fan, M. Zeng, X. B. Lu, X. S. Gao, M. H. Qin, and J.-M. Liu, Optically controlled ultrafast dynamics of skyrmion in antiferromagnets, *Phys. Rev. B* **107**, 214429 (2023).
- [47] S. Mallick, P. Ye, W. Boutu, D. Gauthier, H. Merdji, M. Bibes, M. Viret, K. Bouzehouane, and V. Cros, OAM Driven Nucleation of Sub-50 nm Compact Antiferromagnetic Skyrmions, *Adv. Funct. Mater.*, 2409528 (2024).